JrnlID 12217_ArtID 9376_Proof#1 - 08/06/2014

Microgravity Sci. Technol.
DOI 10.1007/s12217-014-9376-y

ORIGINAL ARTICLE

Comparative Analyses of Esa, Nasa and Jaxa Signals of Acceleration During the Sodi-ividil Experiment

Nuria Sáez · Xavier Ruiz · Fina Gavaldà · Valentina Shevtsova

Received: 22 October 2013 / Accepted: 3 June 2014

Abstract The present work aims to complete the analysis of the vibrational impact generated by the Influence of VIbrations on DIffusion of Liquids, IVIDIL, experiment in a global way. To do so, we have analysed all the episodes which, along the active period between September 2009 and January 2010, accounts for simultaneous accelerometric signals coming from the Columbus (ESA) module, the Destiny (NASA) module and the Pressurized module of the Kibo complex, PM-Kibo, (JAXA) respectively. Signals have been downloaded thanks to the NASA Principal Investigator Microgravity Services, PIMS, website. Vibrational analysis involved the consideration of second and higher order statistical techniques. In addition, a comparative study of the RMS acceleration integrated over one-third octave frequency bands enabled to check if the ISS vibratory limit requirements are everywhere accomplished. In summary it can be concluded that, in the vibratory regime, the experiment in the Columbus module is isolated enough of the Destiny and PM-Kibo ones. In addition, concerning only the Columbus data, the study also concluded that the peculiar energy exchange detected between the nominal frequency of the movement and its third harmonic is due to nonlinearities probably originated by the shaker, the module of translational arrangement mounted on the SODI instrument.

All these results introduce an interesting generic question: is it always correct to consider that the accelerometric data only coming from one module can offer to the Space Station customers a suitable global scenario of the ISS environment?, if not, what is the real extent of these data?

Keywords Acceleration analysis · Microgravity · Bispectrum · Trispectrum

Introduction

An important objective of the International Space Station is to supply a quiescent environment to carry out a wide spectrum of scientific experiments under good enough quality levels of microgravity (DeLombard et al. 2005; Tryggvason et al. 2001). However, the unavoidable daily activity in the Station could appreciably impact on the experiment quality. Inversely, motorized experiments as the present one, in which a translational vibration of the test cell is needed, could be unexpected sources of contamination, not only of the experiments themselves but also of other close simultaneous ones. To gain experience in order to plan corrective damping strategies (Worton 2004; Heese et al. 2004), the degree of propagation of any kind of disturbance is an interesting generic question to be considered mainly in the vibrational range (0.01 - 300 Hz) (Jules et al. 2004). Remember that because in this range the propagation cannot be predicted analytically, it must be investigated experimentally (Hrovat et al. 2004; Hrovat et al. 2012).

The IVIDIL experiment assembled inside the SODI instrument was installed by the ISS expedition 21 within the

N. Sáez · X. Ruiz · F. Gavaldà (✉) · V. Shevtsova
Departament de Física Química i Inorgànica,
Universitat Rovira i Virgili, Marcellí Domingo s/n,
Tarragona, 43007, Spain
e-mail: fina.gavalda@urv.cat

N. Sáez
e-mail: nuria.saez@urv.cat

X. Ruiz
e-mail: josepxavier.ruiz@urv.cat

V. Shevtsova
e-mail: vshev@ulb.ac.be

Glovebox rack -in the Columbus module- (Shevtsova 2010; Shevtsova et al. 2011; Sáez et al. 2013b). The experiment began October 2009 and finished January 2010. During this period about fifty runs were successfully completed. Many of them used a translational motor which shakes the IVIDIL test cell at different frequencies and amplitudes. To complete previous reports (Sáez et al. 2013b; Sáez et al. 2013c) the objective of the present work is to focus on the propagation of the shaker disturbances in the vibrational range. This implies to extent the operational research to all nearest modules able to generate simultaneous accelerometric information, in particular, the ESA Columbus -SAMSes es08 sensor-, NASA Destiny -SAMSII 121f03 sensor- and JAXA PM-Kibo -SAMSII 121f05 sensor- ones. At this respect, it is important to mention that the SAMSes es08 sensor was located in the Glovebox rack, inside the Columbus module, near but not on the experiment. So, there was a small distance between the experiment itself and the sensor.

Even though the above-mentioned simultaneity is very difficult to be achieved, we have detected three episodes all along the life of the experiment labelled as Run 28R, 30R and 33R. The first one, the Run 28R, was active from 13th to 14th of January 2010 and corresponds to a shaking state of 2 Hz of frequency and amplitude of the translational movement of 52 mm. The second Run 30R was active between January 18th and January 19th of 2010 and corresponds to a shaking state of the same frequency but higher amplitude of 62 mm. Finally the third episode, the so-called Run 33R, was active between 15th and 16th January of 2010 and corresponds to a quiescent state in which the motor was switched off. It is also very interesting to have a clear idea of the background, without shaker, for comparison purposes. All accelerometric files were downloaded thanks to the NASA Principal Investigator Microgravity Services (PIMS website; PIMS 2004).

Second order statistical analysis involves the consideration of relevant statistical properties of the signals in both, time and frequency domains. In order to know if the disturbances produced by the SODI shaker significantly alter the ISS vibratory limit requirements (Rogers et al. 1997), RMS values have also been evaluated. Finally, to investigate the nonlinear peculiarities of the shaker disturbances in the present vibrational range, here up to 200 Hz, high order statistical analysis -in particular, the bi and trispectra- have also been considered.

Numerical Procedures

The accelerometric signals are sampled at 500 Hz and properly filtered with a cut-off frequency of 200 Hz. The gain of the sensor located in the ESA Columbus module is 8.5 while that the gain of the other two sensors located in the NASA Destiny and JAXA PM-Kibo modules are 10. The length of each signal is about 18 hours, the same duration as each complete IVIDIL's run. Data units are in g and in order to eliminate possible instrument bias we have systematically demeaned all the raw signals before attempt any mathematical manipulation. The positions and locations/orientations of the SAMS sensors against the International Space Station Absolute coordinate system (SSA: X_A, Y_A, Z_A) are detailed in Fig. 1 and Tables 1 and 2 (Jules et al. 2005). Hereafter we will always use the absolute coordinate system, in this way the X_A direction will coincide with the most relevant direction of the present study, the shaking one (Sáez et al. 2013c).

Time Domain Analysis

A ten seconds interval average acceleration plot is used as a standard representation of long length data files, despite that in this case it must be taken into account that only average tendencies could be detected. The statistical analysis starts with the consideration of the corresponding histograms in order to investigate the kind of distribution associated. Mention here that the Gaussianity is a very important characteristic because nonGaussian distributions would evidence the existence of nonlinearities. To test the Gaussian nature of the signals, the literature offers different strategies, as the presented by Thomson et al. (1997), in which the probability distribution and the fitted Gaussian curve are plotted in logarithmic scale. In the present case we choose another option also very popular in statistics, the quantile-quantile plot, in which the normal behaviour is visualized by a straight line. Additional statistic information is provided by the first quartile, Q1, the third quartile, Q3, the interquartile range (IQR, Q3 - Q1), and the outliers. The outliers here are the percentage of points excluded of the upper, U, and lower, L, whiskers (calculated here as (Q3 + 1.5 (Q3 - Q1)) and

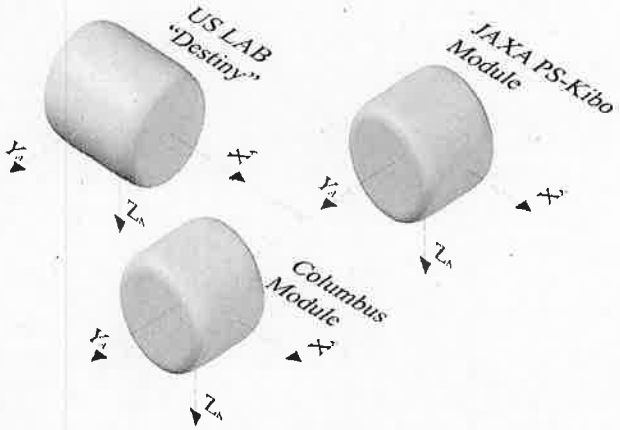

Fig. 1 The International Space Station Absolute coordinate system

Q2

Table 1 SAMS coordinate systems during the experiment

	Location (in)			Orientation (degrees)		
Sensor	X_A	Y_A	Z_A	Roll	Pitch	yaW
ES08	475.71	235.22	160.27	0	90	-90
121f03	191.54	-40.54	135.25	0	30	-90
121f05	466.8	-292.06	214.58	-90	-90	0

(Q3 - 1.5 (Q3 - Q1)), respectively) (McGill et al. 1978; Nelson 1989).

Frequency Domain Analysis

Frequency characterization firstly considers the power spectral density because this positive real function is very illustrative in the understanding of how the power carried out by each signal is distributed in the frequency domain. Hanning windows have been used in all calculations. Based on these calculations and using the Parseval theorem, we also calculate the RMS acceleration level integrated on each one of the thirty-three one-third octave bands between 0.1 and 200 Hz (Rogers et al. 1997). In microgravity, this set of bands is used to define the International Space Station vibratory limits requirements (Jules 2002), that is to say,

$$0.01 \; and \; 0.1Hz; \; a_{RMS} \leq 1.8\mu g \tag{1}$$

$$0.1 \; and \; 100Hz; \; a_{RMS} \leq 18f\,\mu g \tag{2}$$

$$100 \; and \; 300Hz; \; a_{RMS} \leq 1800\mu g \tag{3}$$

being f the value of the centre of the band considered.

Also, to investigate the degree of correlation at each frequency between couples of different signals coming from the three different modules we use the coherence function. This magnitude, similar to the cross-correlation in the time domain, is defined in the frequency domain as the cross-spectral density function of both signals normalized by the product of the corresponding power spectral density functions (Heinnzel et al. 2002).

Table 2 Relationship between the axes from SAMS sensor and the SSA coordinate systems during the experiment

	Unit vector in Analysis Coordinates			
Sensor	Axis	X_A	Y_A	Z_A
ES08	X_{ES08}	0	0	-1
	Y_{ES08}	1	0	0
	Z_{ES08}	0	-1	0
121f03	X_{F03}	0	-0.866	-0.5
	Y_{F03}	1	0	0
	Z_{F03}	0	-0.5	0.866
121f05	X_{F05}	0	0	1
	Y_{F05}	1	0	0
	Z_{F05}	0	1	0

Higher order statistical techniques (Sáez et al. 2013a) are applied to the multimodal distribution records in order to correctly identify the frequency interaction mechanisms that result from the presence of nonlinearities (Kerschen et al. 2006; Hickey et al. 2009). It is important emphasise that if a signal has a Gaussian probability density function then, it has zero polispectra for all the orders higher than two, which corresponds to the power spectrum. The Bispectrum function -third order spectral analysis- is calculated using the direct method as the average of the triple products of Fourier transforms over K segments in which all the records are divided (Collis et al. 1998; Rivola 2000). In the present study, the Fourier transforms are evaluated using 2048 points. Non-overlapping is applied to obtain 14000 Hanning windowed segments corresponding practically to the whole signal. Bispectrum function is a complex magnitude and it can reveal information about the mechanisms which are responsible of quadratic nonlinearities, as for example, the so-called quadratic phase coupling phenomenon, QPC. The power spectrum is a function of one frequency, but the bispectrum depends of two frequencies (f1,f2). A peak in the bispectrum module at (f1,f2) frequencies implies a frequency coupling between f1, f2 and f3 being f1 + f2 = f3. If, in addition, the phase of the bispectrum is zero, a QPC phenomenon is detected (Fackerell et al. 1995a; Fackerell et al. 1995b). This phenomenon indicates that part of the energy associated with the third frequency, f3, comes from the energy of the other two. To check if the biphase is zero, we always use here the biphase histogram method (Sáez et al. 2013a), that is to say, we construct histograms associated to the values of the biphase of each one of the different segments considered only at the corresponding frequency couplings.

Also, from the analysis of trispectrum function -fourth order spectral analysis-, we investigate the presence of cubic nonlinearities in the signals. Similarly as the calculation of the bispectrum function, the trispectrum is evaluated as the average of the quadruple products of Fourier transforms over k segments (Rivola 2000). Here we select 2048 FFT points over 1000 Hanning windowed segments. Trispectrum is a complex magnitude that depends of three frequencies (f1,f2,f3) and it presents many symmetries (Rivola 2000). Here, the module is plotted by drawing spheres at every point in the (f1,f2,f3) space, with a radius proportional to their corresponding modules. Only the maximum values are plotted here and these maxima related four frequencies f1, f2, f3 and f4 being f1 + f2 + f3 = f4 or f1 + f2 - f3 = f4 for the two principal domains. If one point of the trispectrum accomplishes some of these relations simultaneously

with the zero value of the phase of the trispectrum, a cubic phase coupling occurs. Also, the triphase histogram method is applied to check the trispectrum phase at the points where the trispectrum is maximum. (Sáez et al. 2013a)

Results

Figure 2 presents the ten seconds interval average of the X_A acceleration component of the ESA, NASA and JAXA (30R) data. Similar behaviour is exhibited by the other signals (28R and 33R). It can be seen that the acceleration levels are in all cases stable but different. JAXA PM-Kibo module has the lowest acceleration value while that ESA Columbus module has the highest one. A clear perturbation, practically at the end of the run -around the hour fifteen-, is detected in all three subsequent signals but its presence does not significantly affect the subsequent results at all. As mentioned before, we have demeaned all raw signals treated, except the ones reported now in Fig. 2 and Table 3 because we consider illustrative enough to highlight their global characteristics. Hereafter all signals have been demeaned before attempt further manipulations.

The histograms of the X_A acceleration data in the particular case of 30R are shown in Fig. 3. At first glance, the histograms associated to NASA Destiny and JAXA PM-Kibo modules are Gaussian (Figs. 3b and 3c) while that the ESA Columbus one, Fig. 3a, presents a distorted belly shape indicating the lose of Gaussianity. The activation of the shaker seems to be the reason for this breaking of the X_A component -ESA's Y_A and Z_A components remain Gaussians- . In order to quantitatively confirm the Gaussianity, Fig. 4 presents the quantile-quantile plot of each signal. Obviously, X_A accelerometric data of ESA Columbus module, Fig. 4a, does not accomplish this test because the notorious deviations of the curve regarding the straight line corresponding to a normal behaviour. In the other cases, Figs. 4b and 4c, a good correlation is observed except at both ends. The outliers, equivalently the tails of the distributions, slightly distort the complete Gaussian character of the signals. The set of three signals labelled as 28R also present the same tendency. In the case of 33R signals, when the shaker is off, a Gaussian behaviour is confirmed for all the signals.

Table 3 Basic descriptive statistics of the signals

Signals	Mean (mg)	Median (mg)	IQR (mg)	Outliers (%)
ESA 28R	0.3538	0.3437	0.9848	$3.6 \cdot 10^{-5}$
NASA 28R	-0.0238	-0.0239	0.1294	$5.5 \cdot 10^{-1}$
JAXA 28R	-0.0005	-0.0022	0.0685	$7.9 \cdot 10^{-1}$
ESA 30R	0.3539	0.3519	0.6577	$4.5 \cdot 10^{-3}$
NASA 30R	-0.0288	-0.0239	0.1259	$7.0 \cdot 10^{-1}$
JAXA 30R	-0.0002	-0.0037	0.0741	$6.0 \cdot 10^{-1}$
ESA 33R	0.3538	0.3530	0.0707	$7.7 \cdot 10^{-1}$
NASA 33R	-0.0239	-0.0240	0.1332	$5.0 \cdot 10^{-1}$
JAXA 33R	-0.0003	-0.0017	0.0706	$6.7 \cdot 10^{-1}$

Additionally statistical information is presented in Table 3. ESA Columbus X_A accelerometric signals have a mean around 0.35 mg, which is higher than the mean of the other signals. When the motor is on, the interquartile range (IQR) of ESA Columbus signals are also increased and the percentage of outlier is reduced.

The power spectral densities of the X_A component of 30R signals are displayed in Fig.5. Notice that the scales corresponding to the ordinate axes of the three periodograms are not logarithmic to better appreciate the intensities associated with the different frequencies. The highest intensities that appear in ESA30R Columbus signal are associated with the shaking frequency (f_0 = 2Hz)

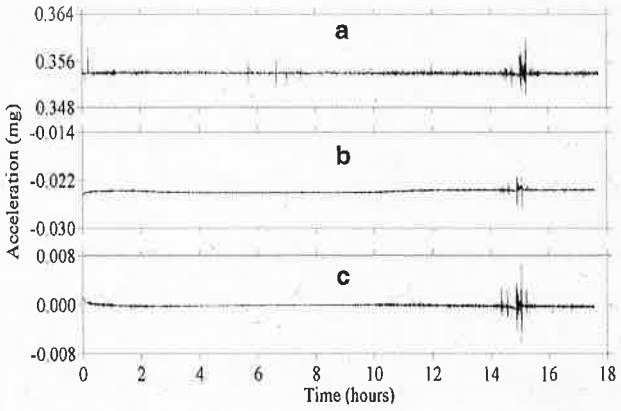

Fig. 2 Ten seconds interval average of X_A components. **a** ESA, **b** NASA and **c** JAXA, 30R signals

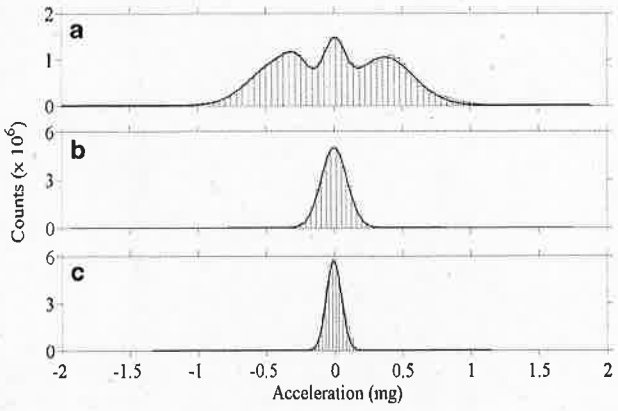

Fig. 3 Histogram of X_A components. **a** ESA, **b** NASA and **c** JAXA, 30R signals

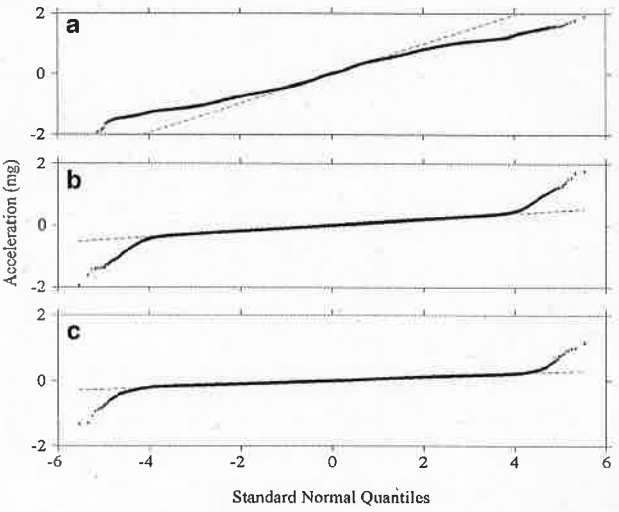

Fig. 4 Quantile-Quantile (Q-Q) plot (X_A components). **a** ESA, **b** NASA and **c** JAXA, 30R signals. The *straight line* corresponds to the normal distribution

and its third harmonic ($3f_0$ = 6Hz). Amazingly the intensity of this harmonic is higher than the corresponding to the fundamental one (f_0). This behaviour indicates that a possible nonlinear mechanism increases the $3f_0$ intensities at the expense of the f_0 one. Tables 4 and 5 quantify all the above mentioned details. From these tables we can see that the shaking and the third harmonic frequencies also appear in the NASA Destiny and JAXA PM-Kibo signals, but the situation is different in both modules. In the case of the NASA Destiny signal the dominant frequencies, 95.4 and 141.7 Hz, could be possibly originated by life support equipment activities. The shaking frequency and the third harmonic are also detected but their intensities are very weak and the third harmonic continues being dominant. On the other hand, the dominant frequency in the JAXA PM-Kibo signal is the third harmonic (6 Hz), the shaking frequency is also appreciable but its intensity is low.

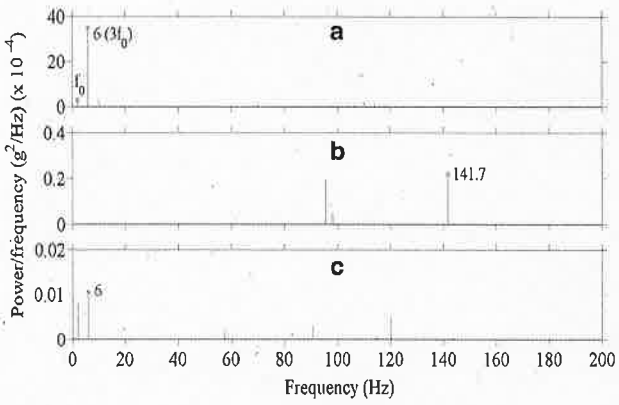

Fig. 5 Power spectral density (PSD) of X_A components. **a** ESA, **b** NASA and **c** JAXA, 30R signals

Table 4 Quantitative power spectral densities results for Run 30R

Frequency(Hz)	Intensity (g^2/Hz) ESA	NASA	JAXA
2	$2.15 \cdot 10^{-4}$	$7.60 \cdot 10^{-9}$	$8.07 \cdot 10^{-7}$
4	$5.60 \cdot 10^{-6}$	–	–
6	$3.50 \cdot 10^{-3}$	$7.14 \cdot 10^{-8}$	$1.05 \cdot 10^{-6}$
8	$1.50 \cdot 10^{-5}$	$5.68 \cdot 10^{-9}$	$6.85 \cdot 10^{-9}$
10	$2.90 \cdot 10^{-4}$	$1.10 \cdot 10^{-8}$	$1.64 \cdot 10^{-9}$
12	$7.89 \cdot 10^{-8}$	–	$3.34 \cdot 10^{-10}$
14	$2.04 \cdot 10^{-5}$	–	$2.92 \cdot 10^{-9}$
18	$2.22 \cdot 10^{-5}$	–	$3.02 \cdot 10^{-10}$
22	$7.76 \cdot 10^{-6}$	–	$7.27 \cdot 10^{-9}$
26	$1.21 \cdot 10^{-5}$	–	–
57.4	–	–	$1.81 \cdot 10^{-7}$
73.1	3.2010^{-6}	–	–
90.5	–	–	$3.09 \cdot 10^{-7}$
95.4	–	$1.95 \cdot 10^{-5}$	–
98.24	–	$5.50 \cdot 10^{-6}$	–
114.7	–	–	$6.68 \cdot 10^{-8}$
120.1	–	–	$5.29 \cdot 10^{-7}$
141.7	–	$2.19 \cdot 10^{-5}$	–
153.7	–	$6.23 \cdot 10^{-9}$	–

The coherence functions for 30R signals are shown in Fig. 6. The NASA and JAXA couple (Fig. 6c) presents a strong correlation around 2 and 6 Hz. The X axes are restricted to the interval 0-50 Hz in order to clarify, as much as possible, the plot contents. For the other cases the maximum value of coherence, only located at 2 Hz, drastically decreases. This fact suggests that the mechanical couplings between ESA - NASA and ESA - JAXA modules are weak. Anyway, the nominal frequency of the shaker, 2 Hz in the present cases, is always transmitted to the neighbour modules.

Table 5 Dominant frequencies and their intensities

Signals	f_0 / Ampl. (Hz) / (mm)	Max. freq. (Hz)	Intensity (g^2/Hz)
ESA 28R	2 / 52	6	$1.6 \cdot 10^{-2}$
NASA 28R		141.7	$2.8 \cdot 10^{-5}$
JAXA 28R		6	$6.0 \cdot 10^{-6}$
ESA 30R	2 / 62	6	$3.5 \cdot 10^{-3}$
NASA 30R		141.7	$2.3 \cdot 10^{-5}$
JAXA 30R		6	$1.0 \cdot 10^{-6}$
ESA 33R	0 / 0	73.1	$7.3 \cdot 10^{-6}$
NASA 33R		141.7	$2.2 \cdot 10^{-5}$
JAXA 33R		90.5	$6.0 \cdot 10^{-7}$

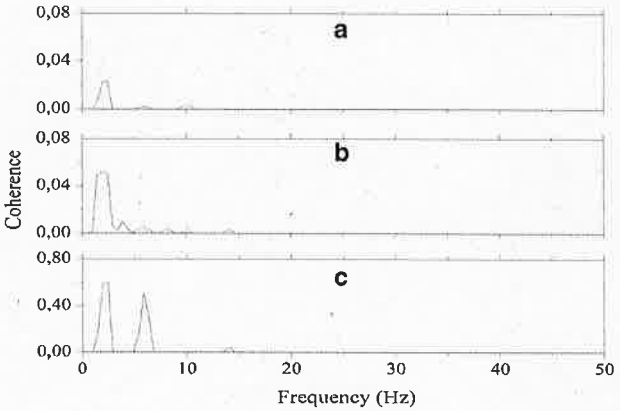

Fig. 6 Coherence functions: **a** ESA-NASA, **b** ESA-JAXA and **c** NASA-JAXA

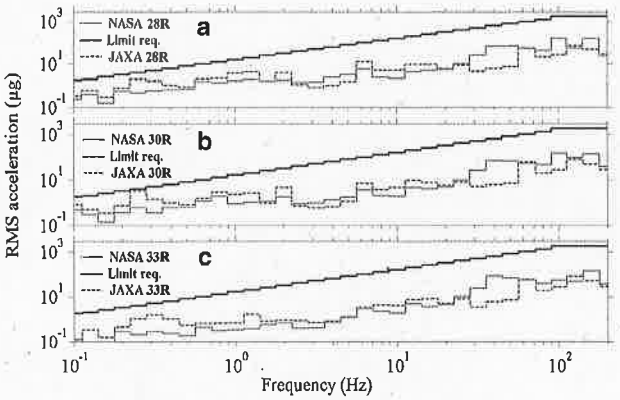

Fig. 8 RMS acceleration vs. one third octave frequency bands. *Bold line* is the ISS vibratory limit requirements

Figure 7 shows the RMS acceleration of the ESA Columbus signals as a function of the one third octave frequency band for the three different days considered. Thick line corresponds to the ISS vibratory limit requirements. We can see that, the RMS levels increase when the shaker is on, cases (a) and (b), and, in these cases, clearly exceed the limit allowed for the frequency bands containing the values of the shaking and its third harmonic. Mention that the existence of relevant RMS values in the above-mentioned bands have also been detected in several preliminary ground test reports. Comparing the curves Figs. 7a and 7b, a good reproducibility of the mechanical conditions is observed, independently of the experiment day. Also, a more detailed inspection shows small changes around the $5f_0$ frequency bands.

Figure 8 presents the RMS acceleration levels of NASA and JAXA PS-Kibo modules. All values are always significantly lower than the corresponding ISS limits, and for low frequencies, minor than 20 Hz, JAXA values are bigger than NASA ones. Mention also, the high RMS values associated with the frequency band containing 0.25 Hz principally in ESA and JAXA signals and mostly in Run 30R (Figs. 7b and 8b). This is probably due to structural movements of the Station itself.

In order to analyze the nonlinear energy exchange between the nominal frequency and its third harmonic it is mandatory to study the bispectrum and trispectrum functions, which are shown in Figs. 9 and 10, respectively. Both figures have been built using also the X_A accelerometric component of the ESA 30R run. Note that Fig. 9 shows redundant information because it appears two symmetric regions against the diagonal line as the symmetry axis (Courtney et al. 2010) and thus we will only consider the peaks located within the lowest triangle region. So, the principal bispectrum peaks that appear in this figure are located at the frequency pairs a:(4,2), b:(6,2), c:(6,4) and d:(10,6). We focus our attention in the first pair, which corresponds to an interaction between the shaker frequency and

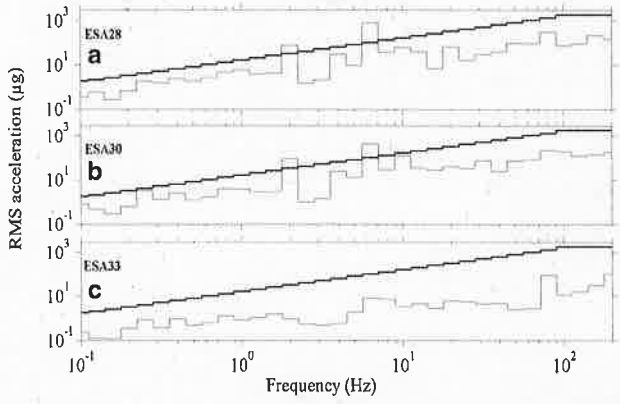

Fig. 7 RMS acceleration vs. one third octave frequency bands. *Bold line* is the ISS vibratory limit requirements

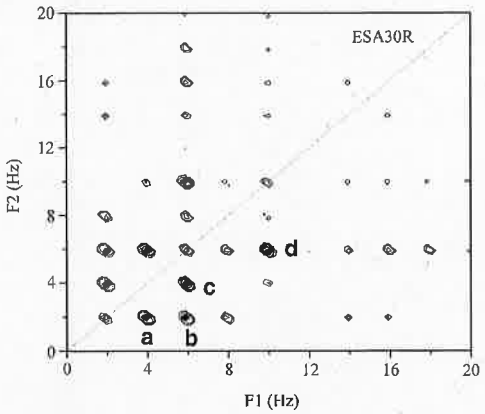

Fig. 9 ESA30R bispectrum. **a** (4,2), **b** (6,2), **c** (6,4) and **d** (10,6)

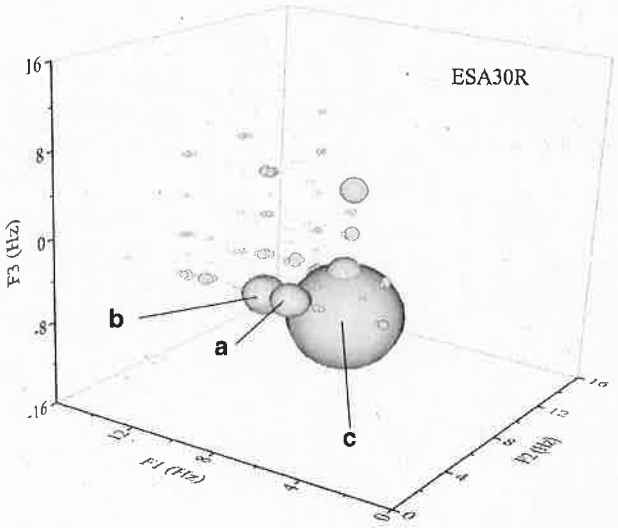

Fig. 10 ESA30R trispectrum. **a** (6,2,-2), **b** (10,6,-6) and **c** (6,6,-6)

its second harmonic, because its addition, 2 + 4 = 6 Hz , could explain the power increase associated to the third harmonic. To investigate if there are quadratic phase coupling at the mentioned pair, we also must check if its biphase accomplishes the condition of zero value. A detailed study of the biphase passing through the construction of biphase histograms has been made (Sáez et al. 2013a), and the results establish that, in the present case, this condition is not accomplished not only for (4,2) pair but either by the others principal pairs. So, the anomalous exchange of energy between the first and third harmonic is not a consequence of a quadratic phase coupling. Therefore we increase one spectral order analyzing the trispectrum function. Results are presented in Fig. 10. Only the triplets with the largest trispectrum values are plotted in this figure. We can see that the maximum trispectrum value is located at c:(6,6,-6) Hz. Another relevant triplets are a:(6,2,-2) and b:(10,6,-6). As before, only (6,6,-6) and (6,2,-2) triplets accomplish that 6 + 6 - 6 = 6 and 6 + 2 - 2 = 6. With the aim of testing if a cubic phase coupling behaviour appears, it must be additionally investigated the existence of phase coupling (triphase must be zero). Also using the histogram phase method, we find that the three triplets have zero triphase value. This result indicates that the third harmonic (6 Hz) increase its energy from itself (6,6,-6), in resonant form, and from the energy of 2 Hz (6,2,-2), while the triplet (10,6,-6) interacts with the fifth harmonic (10 Hz). So, these results indicates that the nonlinearities exhibited in the mechanical device are of cubic type. The literature shows that a possible explanation of this behaviour could be associated to a malfunction of the shaking motor due a misalignment of the axis rotor during the experiment (Sinha et al. 2013).

Conclusions

A comparative analysis of simultaneous accelerometric signals coming from three different modules of the ISS is carried out. The signals correspond to a complete SODI - IVIDIL experiments in which the shaker is switched on or off respectively. Our results clearly show that the shaker breaks the Gaussianity of the ESA Columbus module signal only in the shaking direction, but maintains the Gaussian behaviour of the three components of acceleration in the rest of modules. The shaker frequency (2 Hz) and its third harmonic (6 Hz) dominate the spectral response in the ESA Columbus and in the JAXA PS-Kibo modules. In both modules the power spectrum intensity of third harmonic is higher than the fundamental one. In the case of NASA Destiny, the above-mentioned frequencies are also detected but the highest intensities are presumably related with frequencies associated to life support equipment activities. High values of the coherence function are only found between the NASA Destiny and JAXA PS-Kibo signals at 2 and 6 Hz. In the other cases, a peak is detected at the shaker fundamental frequency but its value is very low. The results also show that the disturbances produced by the mobile mechanical device in the ESA Columbus module do not accomplish the ISS vibratory limit requirements. Finally, high order spectral analysis demonstrate that the peculiar energy exchange between the shaking and the third harmonic frequencies is due to a cubic nonlinear behaviour, probably caused by misalignment of the axis rotor of the shaker.

Concerning the question posed in the Abstract and taking into account the conclusions of the present study say that the mechanical environment of one experiment could not be characterized considering only the records of acceleration from the accelerometers of only one module, especially if the experiment is not there. The researchers need additional information from different modules to adequately characterize the mechanical environment of their experiments. But still, the correlation between experiment and mechanical vibrations is not fine enough, so, the best strategy is to locate accelerometers inside the experiment or, as near as possible -then, taking the corresponding preventions-. But even in this case and, specially in motorized experiments as the present one, the researcher must be very cautions with the choice of the accelerometric information to be correlated with the experimental results, taking into account not only the nominal frequencies associated with the experiment, but also the ones associated with the signal of acceleration obtained during the experiments.

Acknowledgements The present work is part of our participation in the HSF-US/2010-042 and HSF-US/2010-041 ESA projects.

References

Collis, W.B., White, P.R., Hammond, J.K.: Higher-order spectra: the bispectrum and trispectrum. Mech. Syst. Signal Pr. **12**(3), 375–394 (1998)

Courtney, C.R.P., Neild, S.A., Wilcox, P.D., Drinkwater, B.W.: Application of the bispectrum for detection of small nonlinearities excited sinusoidally. J. Sound Vib. **329**, 4279–4203 (2010)

DeLombard, R., Hrovat, K., Kelly, E.M., Humphreys, B.: Interpreting the International Space Station microgravity environment. In: Proceedings of the 43rd AIAA Aerospace Sciences Meeting and Exibit, Reno, Nevada (2005). AIAA-2005-0727

Fackrell, J.W.A., White, P.R., Hammond, J.K., Pinnington, R.J., Parsons, A.T.: The interpretation of the bispectra of vibration signals. I.- Theory, Mech. Syst. Signal Pr. **9**, 257–266 (1995a)

Fackrell, J.W.A., White, P.R., Hammond, J.K., Pinnington, R.J., Parsons, A.T.: The interpretation of the bispectra of vibration signals. II.- Experimental results and applications. Mech. Syst. Signal Pr. **9**, 267–274 (1995b)

Heese, J., Moss, L.: ISS payload microgravity control and disturbance predictions. Microgravity Environment interpretation Tutorial (MEIT), Section 19, pp 1–67 (2004)

Heinnzel, G., Rüdigher, A., Schilling, R.: Spectrum and spectral density estimation by the Discrete Fourier Transform (DFT) including a comprehensive list window functions and some new flat-top windows. Max-Planck-Institut für Gravitations Physik, 15–16 (2002)

Hickey, D., Worden, K., Platten, M.F., Wright, J.R., Cooper, J.E.: Higher-order spectra for identification of nonlinear modal coupling. Mech. Syst. Signal Pr. **23**, 1037–1061 (2009)

Hrovat, K.: Analysis techniques for vibratory data, NASA 7th Annual Microgravity Environment Interpretation Tutorial, NASA Glenn Research Center. Ohio Aerospace Institute, Cleveland, Ohio (2004)

Kerschen, G., Worden, K., Vakakis, A.F., Golinval, J.C.: Past, present and future of nonlinear system identification in structural dynamics. Mech. Syst. Signal Pr **20**, 505–592 (2006)

McPherson, K., Keller, J., Kelly, E., Hrovat, K.: The NASA Glenn Research Center/s acceleration measurement and analysis projects support for the International Space Station (ISS), ASTRO 2012, 16th CASI astronautics conference. Quebec City, Canada (2012)

http://pims.grc.nasa.gov/html/ISSAccelerationArchive.html

Jules, K.: Working in a reduced-gravity environment: "A Primer/", Microgravity Environment Interpretation Tutorial (MEIT), Section 2, pp. 1–77 (2002)

Jules, K., McPerson, K., Hrovat, K., Kelly, E.: Initial characterization of the microgravity environment of the international space station: increments 2 through 4. Acta Astronaut **55**, 855–887 (2004)

Jules, K., Hrovat, K., Kelly, E., Reckart, T.: International Space Station Increment-6/8 Microgravity Environment. Summary report (2005). NASA/TM-2005-213896

McGill, R., Tukey, J.W., Larsen, W.A.: Variation of boxplots. Am. Stat. **32**(1), 12–16 (1978)

Nelson, L.S.: Evaluating overlapping confidence intervals. J. Qual. Technol. **21**, 140–141 (1989)

Principal Investigator Microgravity Services. PIMS ISS Acceleration Handbook. NASA Microgravity Science Division / Microgravity Environment Program Glenn Research Center (2004)

Rivola, A.: Applications of higher order spectra to the machine condition monitoring, p. 107. Publ. DIEM, University of Bologna (2000)

Rogers, M.J.B., Hrovat, K., Kelly, E., Reckart, T.: Accelerometer data analysis and presentation techniques, NASA Lewis Research Center, Clevehand. Ohio (1997)

Sáez, N., Gavaldà, Jna., Ruiz, X.: On the vibrational environment of the "Influence of VIbrations on DIffusion of Liquids" experiment. 11th International Conference on Vibrational Problems (ICOVP), Lisbon, Portugal, 9-12 September (2013a)

Sáez, N., Ruiz, X., Gavaldà, Jna., Pallarés, J., Shevtsova, V.: Comparative ISS accelerometric analyses. Acta Astronaut **94**(2), 681–689 (2013b)

Sáez, N., Ruiz, X., Gavaldà, Jna., Pallarés, J., Shevtsova, V., On the accuracy of the interdiffusion coefficient measurements of high temperature binary mixtures under real ISS condition: C. R. Mec. **341**, 405–416 (2013c)

Shevtsova, V.: IVIDIL experiment onboard the ISS. Adv. Space Res. **46**, 672–679 (2010)

Shevtsova, V., Mialdun, A., Melinkov, D., Ryzhkov, I., Gaponenko, Y., Saghir, Z., Lyubimova, Y., Legros, J.C.: The IVIDIL experiment onboard the ISS: Thermodiffusion in the presence of controlled vibrations. C. R. Mec. **339**, 310–317 (2011)

Sinha, J.K., Elbhbah, K.: A future possibility of vibration based condition monitoring of rotating machines. Mech. Syst. Signal Pr. **34**, 231–240 (2013)

Thomson, T.R., Casademunt, J., Drolet, F., Viñals, J.: Coarsening of solid-liquid mixtures in a random acceleration field. Phys. Fluids. **9**(5), 1336–1343 (1997)

Tryggvason, B.V., Redden, R.F., Herring, R.A.: The vibration environment on the International Space Station: Its significate to fluid-based experiments. Acta Astronaut **48**(2-3), 59–70 (2001)

Worton, M.: Fundamentals of microgravity vibration isolation. Microgravity Environment Interpretation Tutorial (MEIT), Section 14, pp. 1–22 (2004)